analytical chemistry

pubs.acs.org/ac Article

A Bio-inspired Extended-Gate Metal-Oxide-Semiconductor Field-Effect-Transistor for Highly Sensitive Amino Acid Enantiodiscrimination

Le Li,[⊥] Jingjing Zhang,[⊥] Haitao Dai, Deyu Cai, Caijun Guo, Yin Xiao,* Xiaofei Ma, and Yong Wang*

Cite This: *Anal. Chem.* 2021, 93, 14425−14431 Read Online

ACCESS | Metrics & More | Article Recommendations | Supporting Information

ABSTRACT: As the most important small molecules revealing the origins of life, amino acids (AAs) play essential roles in living organisms and their facile enantiodiscrimination has long been a great challenge for analytical chemists. Inspired by the specific stereomatching effect between biomolecules and AA enantiomers, herein, we first developed a bio-inspired highly sensitive platform based on an extended-gate metal-oxide-semiconductor field-effect-transistor (EG-MOSFET) for highly sensitive AA enantiodiscrimination. Bovine serum albumin (BSA) was self-assembled on deposited Au surfaces to afford the extended gate (EG) sensing unit, and its enantiorecognition ability was initially verified using common electrochemical techniques. The EG was thereafter installed to a MOSFET to build the desired BSA-EG-MOSFET highly sensitive chiral sensing platform, which realized the efficient enantiodiscrimination of essential AAs with high sensitivity, where effective chiral resolution was achieved at the femtomole level to phenylalanine (Phe). Combining molecular docking and circular dichroism spectroscopy, the weak intermolecular interactions between BSA and AAs enantiomers were investigated and the mechanism for signal amplification was proposed. Our results demonstrate that the as-fabricated biosensor has great potential in highly sensitive chiral sensing fields and can also afford a potential tool for biomolecular interaction investigations.

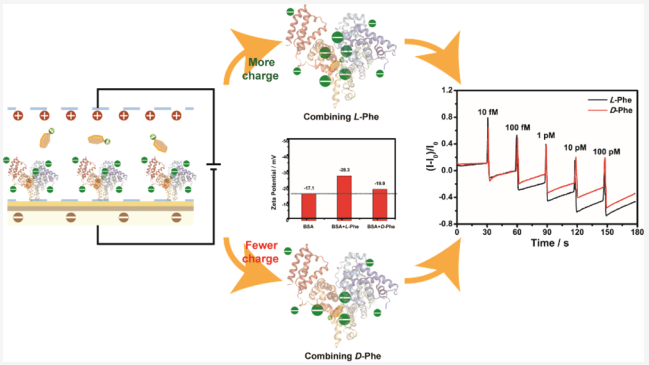

The origin of homochirality in life is a fundamental mystery. Amino acids (AAs), as the basic building block of life, participate in various physiological activities and play essential roles in living organisms; therefore, the development of facile and efficient AA enantiodiscrimination methodologies has attracted great attention in both analytical and biological chemistry. Currently, the chiral resolution of AA enantiomers is generally achieved by high-performance liquid chromatography,[1] circular dichroism spectroscopy,[2] and electrochemistry and nuclear magnetic resonance,[3,4] which are often time-consuming, cost-ineffective, or poorly sensitive. Hence, there is a remarking requirement to develop label-free, rapid, and highly selective and sensitive AA enantiorecognition devices.

Field-effect transistors (FETs) have been widely demonstrated as an ideal candidate for a rapid and sensitive sensing platform for diverse guests such as gases, glucoses, or biomarkers profiting from their amplification ability.[5−12] However, highly sensitive chiral sensing FET devices are still in the exploration stage since the two enantiomers possess identical charge and the enantioselective interactions are always very weak. In our previous work,[13−16] organic field-effect transistors (OFETs) have been successfully used as the sensing platform to realize the identification and quantification of some enantiomers with cyclodextrin derivatives as chiral media. The use of thin film organic semiconductor active layers endows OFETs great potential in the field of flexible sensing. However, their complex preparation process limits their development and practical applications.[17] Also, since the sensitive layer was decorated on the semiconducting layer, cumbersome waterproof treatment was essential to avoid fatal deterioration of the semiconductors in the solution environment.[18] Devices composed of metal-oxide-semiconductor structures have the advantages of miniaturization and parallel sensing[17,19] Alternatively, sensors based on the extended-gate metal-oxide-semiconductor field-effect-transistor (EG-MOSFET) have advantages of an easy fabrication process and high stability and reproducibility, where the sensing materials locate on the EG electrode apart from the semiconductor. Iskierko et al. recently designed a molecular imprinted polymer recognition unit for enantioselective determination of phenylalanine (Phe) using an EG-MOSFET with a detection limit of

Received: June 10, 2021
Accepted: October 15, 2021
Published: October 21, 2021

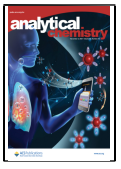

13 μM, which reveals the great potential of the EG-MOSFET in chiral discrimination.[20]

On a separate note, natural biological macromolecules such as proteins have interesting chiral preference. For example, bovine serum albumin (BSA) has a free sulfhydryl group for easy loading and the three helical domains arranged in the shape of the heart can give full play to its stereo recognition ability.[21] Based on the inherent chiral selectivity of BSA, it has been widely used in chromatography or capillary electrophoresis enantioresolution as well as electrochemical chiral recognition.[21−28] However, ascribed to the instrumentation limitation such as high cost, tedious operation, high detection limit, and easy devitalization of BSA, traditional chromatography and sensing techniques hardly meet the increasing requirements for fast and facile discrimination of low-concentration essential AAs. Therefore, considering the weak interactions between such biological molecules and low-concentration chiral analytes, versatile and efficient sensing methodologies involving efficient signal amplification are highly expected in this research field.

Herein, inspired by the stable sensing and the signal amplification characteristics of the EG-MOSFET, the stable bonding ability between BSA and gold,[29,30] and the natural chiral matching effect of BSA, we constructed an EG-MOSFET researching platform by simply combining single-layer BSA-sensitized Au with a MOSEFT. This robust bio-inspired sensing approach afforded a rapid and highly sensitive chiral recognition ability toward five essential AAs and may serve as an efficient tool for investigation of weak steric interactions between AAs and biomolecules combining with molecular docking and circular dichroism (CD).

EXPERIMENTAL SECTION

Materials. Bovine serum albumin (BSA), D-tryptophan (D-Trp), L-tryptophan (L-Trp), L-phenylalanine (L-Phe), D-phenylalanine (D-Phe), L-lysine (L-Lys), D-lysine (D-Lys), L-methionine (L-Met), D-methionine (D-Met), L-threonine (L-Thr), and D-threonine (D-Thr) were purchased from Aladdin Chemistry Co., Ltd. (Shanghai, China). KCl, $K_3Fe(CN)_6$, $K_4Fe(CN)_6$, and other chemicals not mentioned were received from Sinopharm Chemical Reagent Co., Ltd. All aqueous solutions were prepared with ultrapure water (Milli-Q, Millipore). Polydimethylsiloxane (PDMS) was purchased from Center Qiheng Scientific Instrument Co., Ltd. (China). Acetone, anhydrous ethanol, and isopropanol were obtained from Rianlon Corporation (Tianjin, China). Phosphate-buffered solution (PBS) was purchased from Shanghai Beyotime Biotechnology Co., Ltd.

Preparation of BSA-EG. To fabricate the extended-gate electrode, a gold thin film (80 nm thickness) was deposited on a glass substrate by thermal evaporation. The gold electrode was washed sequentially in acetone, anhydrous ethanol, isopropanol, and DI water and then dried in a nitrogen stream. A 10 $mg{\cdot}mL^{-1}$ BSA solution (10 mM PBS solution, pH 7.2) was prepared, and the EG electrode was soaked in the substrate solution at 4 °C to prepare a protein-sensitized electrode.

Characterization. The optical activity of L-/D-Phe + BSA, L-/D-Thr + BSA and BSA was characterized by J-810 circular dichroism (CD, JASCO, Tokyo, Japan). Samples were prepared with 10 mM PBS to provide a protein−amino acid complex with a molar ratio of 1:1. A 1 mm optical length quartz cell was used to obtain the 180−250 nm spectra at room temperature in a nitrogen atmosphere. Each spectrum presented was the average of three consecutive scans at a scan speed of 200 $nm{\cdot}min^{-1}$ and a bandwidth of 2 nm. X-ray photoelectron spectroscopy (XPS) was performed by using a PHI 5000 Versa Probe (Kanagawa-ken, Japan). The hydrophilicity was evaluated by a POWEREACH JC2000D1 contact angle measuring instrument (Shanghai, China). Cyclic voltammogram (CV) was recorded over the potential range from −0.2 to +0.6 V at a scan rate of 20 $mV{\cdot}s^{-1}$, and the Nyquist plots were recorded in the same solution in the frequency range from 10^5 to 10^{-2} Hz. The differential pulse voltammogram (DPV) was recorded in the potential range of −0.2 to +0.6 V, under default parameters. All electrochemical measurements were carried out in a conventional three-electrode cell with a 0.1 M KCl solution containing 5 mM $[Fe(CN)_6]^{3-/4-}$ using a CHI-650E electrochemical workstation (Shanghai Chenhua Instruments Co., China). The counter electrode was a platinum wire and a KCl-saturated calomel electrode (SCE) was selected as the reference electrode. A gold-plated glass (1.0 × 1.0 cm) or a modified gold-plated glass (BSA-EG) was used as the working electrode. Zeta potential measurements were performed on a Zetasizer nano ZS (Malvern Instruments Ltd., UK). The concentration of protein was 1 mg/mL. The molar ratio of protein to amino acid was 1:0.5. The dispersant was deionized water and the temperature was 25 °C. Proton nuclear magnetic resonance (^{1}H-NMR) spectra were collected on a JNM-ECZ600R/S1 (600 MHz) supplied by a JEOL (Musashino, Akishima, Tokyo). The concentration of BSA was 0.4 mM and the Phe isomer was 20 mM in 10 mM phosphate-10% D_2O buffer. The crystal structure of BSA was extracted from the RCSB Protein Data Bank (PDB-ID: 4OR0). The 3D structures of D-Phe, L-Phe, D-Thr, and L-Thr were extracted from the ZINC database according to their ZINC-ID (ZINC-ID: ZINC1927, ZINC105196, ZINC895399, ZINC895103). The four structures were separately and manually placed into the active site of BSA. The conformation with the minimum binding energy was considered as the BSA-bound conformation. The binding energy is calculated based on the sum of the intermolecular energy and total internal energy, in which the intermolecular energy includes van der Waals force, hydrogen bond, desolv energy, and electrostatic energy. All docking simulations were performed using AutoDock 4.0.

FET Sensing Procedure. The electrical characteristics of the FETs were measured by Keithley 2400 SCS under ambient conditions. Stock solutions of analytes were prepared with 1% PBS and filtered through a syringe filter (pore size 0.22 μm) before use. The EG electrode and MOSFET were connected by wire clip and the gate voltage was applied through the copper wire. For non-real-time detection, a PDMS cell fabricated on the EG electrode was used to contain the analyte solution. Sample solution was pipetted to the modified extended gate electrode and allowed to stand for 30 s. The electrical characteristics of the sensor were measured under the condition of $V_{GS} = V_{DS} = 1.2$ V. In real-time testing, 1% PBS was added as the electrolyte to PDMS cell to establish a baseline. Then, enantiomer solution in 1% PBS electrolyte was sequentially delivered to the PDMS cell. The time interval of each concentration delivery was about 30 s.

RESULTS AND DISCUSSION

XPS Analysis and Water Contact Angle Characteristics. The successful assembly of a BSA single layer on Au was

https://doi.org/10.1021/acs.analchem.1c02460
Anal. Chem. 2021, 93, 14425−14431

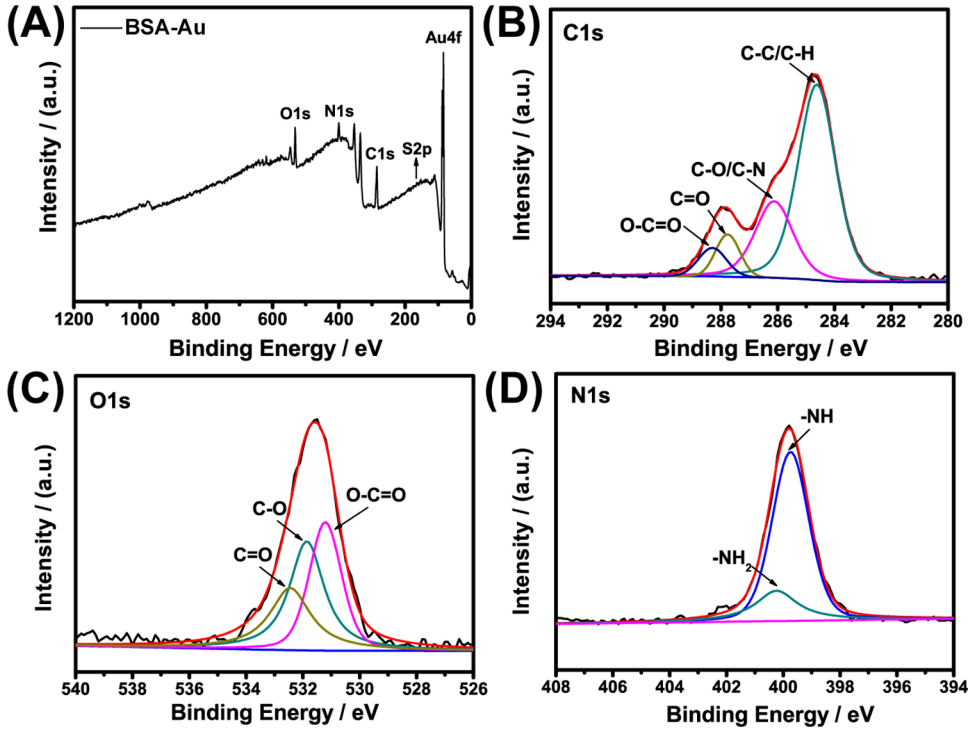

Figure 1. XPS (A) survey spectra, C1s (B), O1s (C), and N1s (D) regions for the BSA-modified Au surface.

initially verified by XPS (Figure 1A). As presented in Figure 1B, the C1s spectra was fitted into four main components with binding energies of 284.6, 286.1, 287.7, and 288.3 eV, corresponding to the C−C, C−N, C═O, and O−C═O of BSA, respectively.[31] In the N1s peak and O1s peak, O═C (532.4 eV), O−C (531.8 eV), O−C═O (531.2 eV), −NH (399.8 eV), and $-NH_2$ (400.2 eV) can be observed in Figure 1C,D.[32] The contents of each element are summarized in Table S1. The change in water contact angle also indicates that the BSA is successfully loaded. The water contact angle on bare Au (83.73°) is decreased to 72.83° after being immobilized with hydrophilic BSA (Figure S1). AFM showed that the surface roughness of the gold electrode after BSA treatment decreased from 1.51 to 1.16 nm, indicating that the BSA load on the gold electrode surface was relatively uniform. The thickness of BSA on the gold electrode surface is estimated as ∼2.7 nm, which means that BSA is adsorbed as a monolayer (Figure S2).

Electrochemical Properties of BSA-EG. The chiral discrimination ability of the BSA-modified Au was evaluated by CV and DPV using Phe as the model analyte. As shown in Figure 2A, decreased currents of the $[Fe(CN)_6]^{4-/3-}$ redox pair are observed for the BSA-Au electrode compared to bare Au because the nonconductive BSA layer blocks the effective charge transfer. The surface coverage of the EG by BSA was estimated by EIS curves fitted with the Randles circuit model (Figure 2B). According to eq 1, the surface coverage (θ) of BSA on Au was determined as 74.1%,[33] suggesting a high and compact surface coverage.

$$\theta = 1 - \frac{R_{ct}^{0}}{R_{ct}} \quad (1)$$

where R_{ct} and R_{ct}^{0} are the charge transfer resistances for BSA-EG and bare EG, which were determined as 141.5 and 36.7 Ω, respectively.

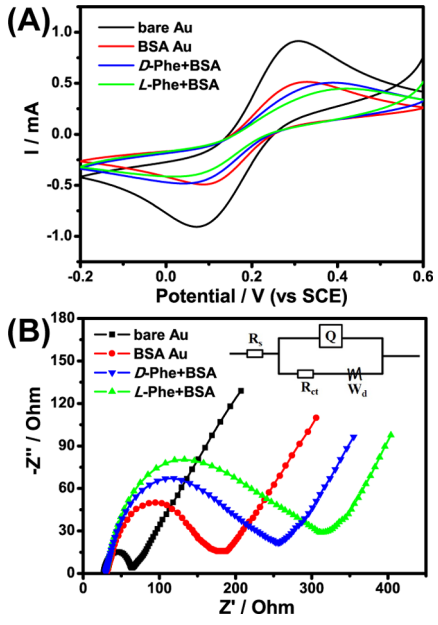

Figure 2. CV (A) and Nyquist plots (B) in the electrolyte (5 mM $[Fe(CN)_6]^{4-/3-}$, 0.1 M KCl) containing 5 mM L- and D-Phe. Scan rate of CV, 20 $mV \cdot s^{-1}$; frequency range of Nyquist plots, 10^5 to 10^{-2} Hz. Inset of (B) is the equivalent circuit.

In the presence of Phe, the peak current decreased more significantly for the L-enantiomer than that of the D-enantiomer, which is consistent with the change tendency of R_{ct} (R_{ct}^{L} = 264.3 Ω, R_{ct}^{D} = 209.5 Ω). This result reveals that the interaction between L-Phe and BSA is stronger than that of D-Phe.[34] The difference of the cathodic peak current ($\Delta I = I_L - I_D$) between the L- and D-isomer was determined as −54.7 μA, indicating the effective chiral recognition ability of the as-prepared BSA-EG. DPV was employed to further estimate the

https://doi.org/10.1021/acs.analchem.1c02460
Anal. Chem. 2021, 93, 14425−14431

detection range and LOD of the BSA-Au electrode for Phe. The bare gold electrode lacks chiral recognition sites and cannot recognize amino acid enantiomers (Figure S3). As shown in Figure 3A,B, a declined current was observed as the

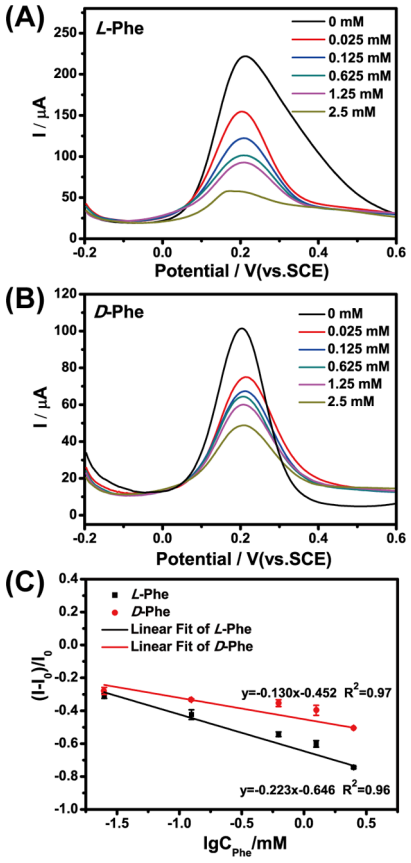

Figure 3. Differential pulse voltammograms of L-Phe (A) or D-Phe (B) in the range of 0.025−2.5 mM and calibration plot of peak current versus logarithmic concentration of Phe isomers (C).

increment of enantiomer concentration for both L- and D-isomers. A satisfactory linearity relationship between logarithmic concentration lg c and current change percentage $(I - I_0)/I_0$ was obtained with an R^2 of 0.96 for L-Phe and 0.97 for D-Phe, suggesting a detection range from 0.025 to 2.5 mM BSA-EG as presented in Figure 3C. Accordingly, the LODs were determined as 25.9 μM and 58.7 μM for L- and D-Phe, respectively. It can be obtained by calculation where L- and D-Phe could be enantioselectivity resolved at the 8.2 μM concentration. In addition, the BSA-Au electrode also showed a good recognition effect on Thr enantiomers (Figure S4).

Chiral Sensing of AAs on the BSA-EG-MOSFET. We employed the BSA-Au electrode as the EG to construct a BSA-EG-MOSFET chiral sensor as illustrated in Figure 4A, where the MOSFET was expected to amplify the interaction difference between BSA and each isomer to afford a highly sensitive chiral resolution. It was found that after assembly of BSA, the current is slightly decreased in PBS (pH 7) (red line) compared to bare Au (black line), indicating the BSA negative charge might be exposed in this case, which suppresses the induced charge in the MOSFET semiconductor (Figure 4B). It is exciting to find that the current is significantly reduced via introducing the guesting AA enantiomers and there is a great difference in the response toward aromatic D-Phe (green line)

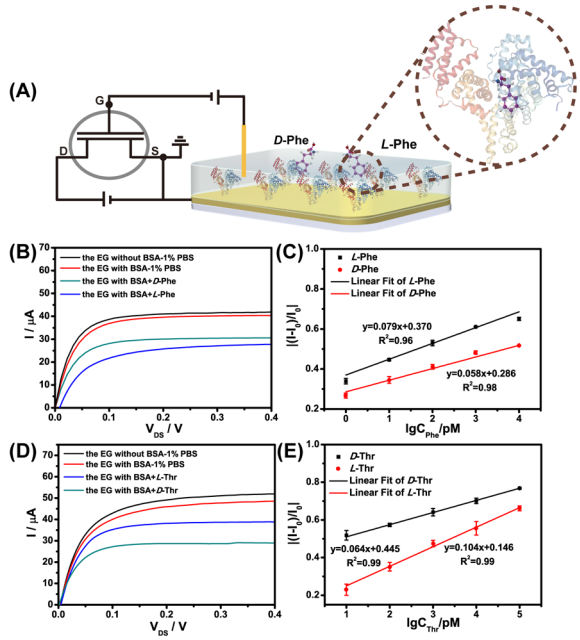

Figure 4. (A) Schematic diagram of the detection device and changes in output current and linear relationship of the BSA-EG-MOSFET by Phe (B, C) and Thr (D, E) at logarithmic concentration in 1% PBS at room temperature.

and L-Phe (blue line). Meanwhile, the same results are also observed with the introduction of alkyl AAs Thr (Figure 4D). For comparison, the bare Au electrode provided no chiral selectivity under the same operating conditions (Figure S5). These results convince the excellent signal transfer and amplification of the BSA-EG-MOSFET. To verify the quantitative capability of the novel sensing platform, we evaluated its response toward different concentrations of Phe and Thr enantiomer pairs. As shown in Figure 4C,E, a good linear relationship is found with both Phe and Thr enantiomers in which the detection limit for Phe was determined as 1.39 fM and for Thr was 0.57 pM, indicating the application reliability of the BSA-EG-MOSFET.

Encouraged by the above interesting results, we performed a real-time chiral sensing for various AAs using the established BSA-EG-MOSFET. We first confirmed that the baseline was reversible when the identical sample was applied (Figure S6). It was exciting to find that the chiral resolution achieved by the BSA-EG-MOSFET for all the testing AAs is in the range of 100 fM−1 nM (Figure 5), which is far beyond the sensitivity (micromolar) of the previous electrochemical method. This result demonstrates that the weak enantioselective interactions between BSA and each isomer at such a low concentration can be effectively transformed to electronic signals and magnified by the as-prepared platform to afford higher chiral sensitivity compared with most of the previously reported performance of chiral FET sensors (Table S2). Generally, the BSA-EG-MOSFET provided better resolution to AAs with aromatic groups (Phe, Trp) than other analytes and the high sensitivity of Thr suggests a positive contribution of the hydroxyl group to the chiral recognition, probably through the formation of hydrogen bonds with BSA. The interactions such as H bonding, $\pi-\pi$, and electrostatic effects between BSA and analytes contribute to the actual protein charging status or conformation resulting in the alteration of the induced charge of semiconductors leading to the sensitive signal output, which

https://doi.org/10.1021/acs.analchem.1c02460
Anal. Chem. 2021, 93, 14425−14431

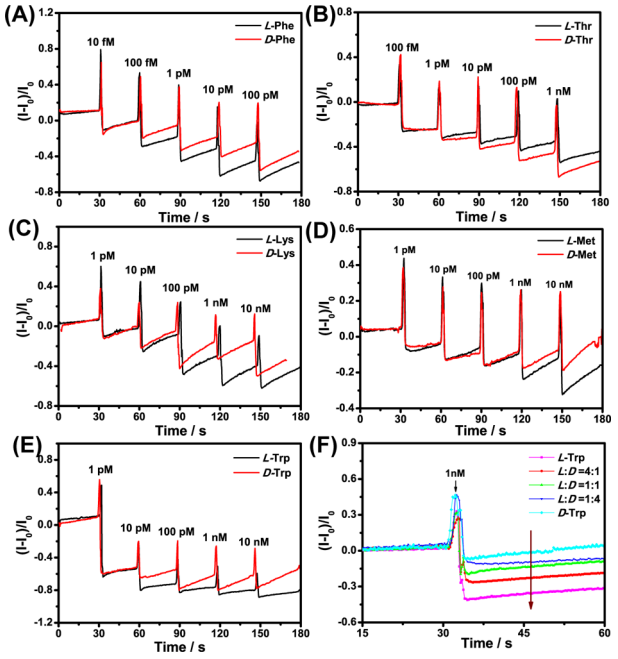

Figure 5. Real-time sensing responses of the BSA-EG-MOSFET to five enantiomer pairs in 1% PBS electrolyte solution ((A) Phe, (B) Thr, (C) Lys, (D) Met, and (E) Trp). Real-time sensing responses of the BSA-EG-MOSFET to 1 nM enantiomer mixtures of Trp (F) at $V_{DS} = V_{GS} = 1.2$ V.

will be discussed in Mechanism Investigation. Also, the BSA-EG-MOSFET is also proven to have the ability to determine the D- and L-isomer content in racemic mixtures at a total concentration of 1 nM (Figure 5F), which suggests its great potential in practical quantitative chiral analysis.

Mechanism Investigation. Considering the relatively low ionic strength (0.1 mM), the charge effect is more dominant than the capacity effect after modification of BSA since the biomolecule charges will locate in the Debye length.[35] As found in the above section, the drain current of the n-type MOSFET decreased due to the negative charge of BSA at pH 7 as shown in Figure 4B,C (black line vs red line). Taking Phe as the model analyte, introduction of Phe enantiomers provides more negatively charged molecules on the gate surface and induces fewer electrons on the p-type substrate (Figure 6A), resulting in the further declined saturated current (Figure 4B, red line vs green line or blue line). BSA on the EG electrode

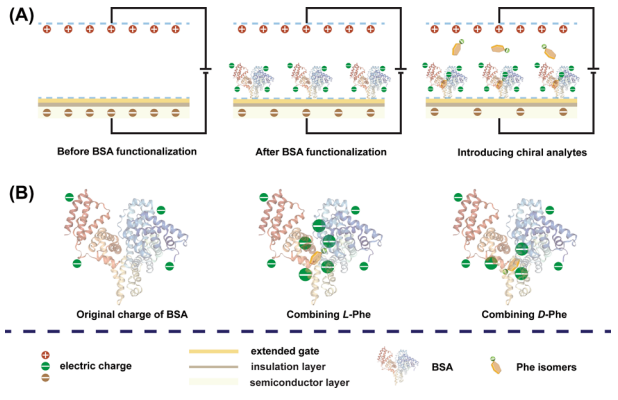

Figure 6. Schematic illustration of the work principle of the BSA-EG-MOSFET. Charge change of EG (A) and charge change of BSA (B).

interacts with the L-isomer to give a more reduced saturated current, which means more negative charge than combining with the D-isomer (Figure 6B). From the change of drain current of the BSA-EG-MOSFET in Figure 4B (blue line vs green line), we can infer that the interactions between BSA and the L-isomer are stronger than that of the D-isomer. This result is supported by zeta potential (Figure S7). When BSA combined with L-Phe, the zeta potential changed from −17.1 to −28.3 mV, but it only changed to −19.9 mV after binding with D-Phe. Consequently, in the case of L-Phe, more mobile cations in the buffer are neutralized by the BSA before reaching the gate electrode surface, which in turn decreases the cation accumulation and hence the distribution of bias voltage at the gate.[36]

.

The above speculation is supported by molecular docking and CD investigation. The docking results are summarized in Table S3 and the dominating configurations of the AA + BSA complex with the lowest binding energy are shown in Figure 7.

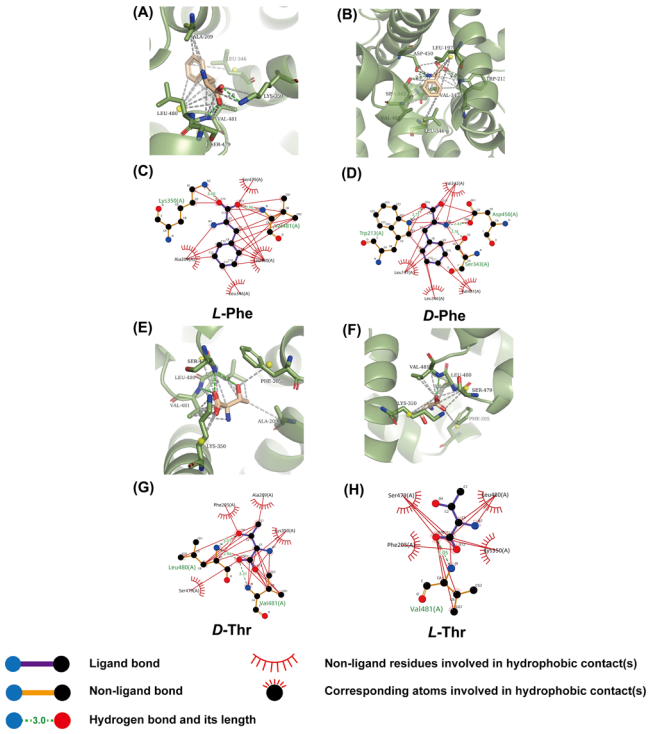

Figure 7. Structure of BSA showing the subdomains and binding sites of Phe (A, B) and Thr (C, D) enantiomers. The 2D diagram shows the interaction between Phe (E, F) and Thr (G, H) enantiomers with the neighboring residues.

As shown in Table S3, the more negative binding free energy (ΔG^0) of L-Phe + BSA compared with *D*-Phe + BSA demonstrates the stronger interaction between BSA and the L-isomer, which is consistent with the larger saturated current change of the BSA-EG-MOSFET induced by L-Phe. The Phe is surrounded by hydrophobic amino acids residues Leu-346, Val-481(L- and D-Phe), Ala-209 (L-Phe), Leu-480 (L-Phe), Leu-197 (D-Phe), and Val-342 (D-Phe), Trp-213 (D-Phe), polar amino acids residues Ser-479 (L-Phe) and Ser-343 (D-Phe), and charged amino acids residues Lys-350 (L-Phe) and Asp-450 (D-Phe), which suggests that the hydrophobic, dipole, and electrostatic interactions between BSA and Phe contribute together to the chiral resolution. Also, hydrogen bonds were

https://doi.org/10.1021/acs.analchem.1c02460
Anal. Chem. 2021, 93, 14425−14431

also found between the carboxylic and amino group of L-Phe with the amino acid residues of BSA.

Importantly, although both L- and D-Phe mainly locate in the hydrophobic cavity in subdomain IIA of BSA as shown in Figure S8A,B, D-Phe entered the cavity more deeply and the obstacle to changing the two-dimensional structure of the protein was more obvious. Moreover, the results of ^{1}H-NMR confirmed the different weak intermolecular interactions between Phe enantiomers and BSA. As shown in Figure S9, after complex formation, the L-Phe proton signals exhibited downfield shifts while D-Phe showed upfield shifts (Figure S9), indicating the different complex confirmation of the two enantiomers with BSA, which is consistent with the molecular docking results shown in Figure S8A,B. L-Phe could be expected to lead to the looser structure of BSA than D-Phe and facilitate the exposure of more amino acids residues, hence resulting in more negative charge on the BSA-EG electrode surface. The comparable conclusion is also applicable to Thr isomers (Table S3, Figure S8C,D).

The CD investigation also proved that introduction of Phe leads to a looser BSA structure with reduced α-helix content, which is more obvious for L-Phe (Figure S10A).[37,38] The correlation between the current change and BSA−enantiomer interactions was also demonstrated with another alky amino acid Thr, where D-Thr results in a more declined saturated current consistent with the stronger D-Thr + BSA interactions and a looser structure of BSA compared to L-Thr (Figure S10B). In summary, the chiral isomers that can interact with BSA more strongly and lead to a looser structure will lead to a larger current variation of the BSA-EG-MOSFET and vice versa, demonstrating that the different interactions between BSA with L- and D-isomers of AAs produce a structure change and hence distinct effective charge change of BSA, which could be sensitively and intuitively reflected by the alteration of the BSA-EG-MOSFET saturated current, hence affording the good chiral sensitivity.

CONCLUSIONS

This work reported the first field-effect transistor chiral sensor with bovine serum albumin-modified Au as the extended gate. The detection platform achieved sensitive discrimination of essential amino acids such as Trp, Phe, Lys, Met, and Thr enantiomers. The difference in the detection limit of phenylalanine fully reflects the unique superiority of using an EG-MOSFET as the detection platform to improve sensitivity. The results of molecular docking and CD results show that the presence of amino acid molecules can significantly respond to the conformation of BSA. The hydrophobic interaction, hydrogen bonds, and electrostatic interaction are the basis for chiral recognition. Therefore, it is easy to understand the different recognition ability of BSA for various AAs. The sensing mechanism is mainly the charge effect and the more negatively charged residues of BSA are exposed, the more significant the change in the bias voltage at the gate, which will eventually lead to varying degrees of current changes. In view of the portability, sensitivity, and universality of such a bio-inspired extended gate FET, we hope that it will gain more and more attention in the field of chiral sensing and chiral interactions. Although the current work provides a satisfied highly sensitive chiral sensing platform, it is still the biggest dilemma in this field that the detection of chiral isomers can so far not be done without knowing the exact concentration or the enantiomeric excess value.

ASSOCIATED CONTENT

Supporting Information

The Supporting Information is available free of charge at https://pubs.acs.org/doi/10.1021/acs.analchem.1c02460.

Content of surface elemental; water contact angle measurements; AFM diagram of the gold electrode surface; differential pulse voltammograms; real-time sensing responses of the Au-EG-MOSFET and BSA-EG-MOSFET; performance summary of the chiral sensor based on the FET; summary of interaction residues, hydrogen bond length, and binding energy of Phe and Thr with BSA; zeta potential of BSA; dominant conformation of the BSA and AA complex obtained from molecular docking; ^{1}H NMR of pure BSA and BSA + AAs (PDF)

AUTHOR INFORMATION

Corresponding Authors

Yin Xiao − *School of Chemical Engineering and Technology, Tianjin Engineering Research Center of Functional Fine Chemicals, Tianjin University, Tianjin 300072, P. R. China;* orcid.org/0000-0001-6582-261X; Email: xiaoyin@tju.edu.cn

Yong Wang − *Tianjin Key Laboratory of Molecular Optoelectronic Science, Department of Chemistry, School of Science, Tianjin University, Tianjin 300354, P. R. China;* orcid.org/0000-0003-4666-2053; Email: wangyongtju@tju.edu.cn

Authors

Le Li − *Tianjin Key Laboratory of Molecular Optoelectronic Science, Department of Chemistry, School of Science, Tianjin University, Tianjin 300354, P. R. China*

Jingjing Zhang − *Tianjin Key Laboratory of Molecular Optoelectronic Science, Department of Chemistry, School of Science, Tianjin University, Tianjin 300354, P. R. China*

Haitao Dai − *Tianjin Key Laboratory of Low Dimensional Materials, Physics and Preparing Technology, Department of Physics, School of Science, Tianjin 300072, P. R. China;* orcid.org/0000-0002-1994-3135

Deyu Cai − *School of Biomedical Engineering and Technology, Tianjin Medical University, Tianjin 300072, P. R. China*

Caijun Guo − *School of Chemical Engineering and Technology, Tianjin Engineering Research Center of Functional Fine Chemicals, Tianjin University, Tianjin 300072, P. R. China*

Xiaofei Ma − *Tianjin Key Laboratory of Molecular Optoelectronic Science, Department of Chemistry, School of Science, Tianjin University, Tianjin 300354, P. R. China;* orcid.org/0000-0001-8047-5193

Complete contact information is available at: https://pubs.acs.org/10.1021/acs.analchem.1c02460

Author Contributions

⊥L.L. and J.Z. contributed equally to this work.

Notes

The authors declare no competing financial interest.

ACKNOWLEDGMENTS

This work was financially funded by the National Key R&D Program of China (2019YFC1905500), the National Natural Science Foundation of China (Nos. 21922409 and 21976131)

and Tianjin Research Program of Application Foundation and Advanced Technology (18JCZDJC37500 and 17JCYBJC20500). Special thanks are given to Dr. Zhang Tao of School of Biomedical Engineering and Technology, Tianjin Medical University for the helpful assistance in dealing with molecular docking.

REFERENCES

(1) Rutkowska, M.; Płotka-Wasylka, J.; Morrison, C.; Wieczorek, P. P.; Namiesnik, J.; Marc, M. *TrAC, Trends Anal. Chem.* **2018**, *102*, 91−102.
(2) Lynch, C. C.; De los Santos, Z. A.; Wolf, C. *Chem. Commun.* **2019**, *55*, 6297−6300.
(3) Guo, L.; Yang, B.; Wu, D.; Tao, Y.; Kong, Y. *Anal. Chem.* **2018**, *90*, 5451−5458.
(4) Hamaguchi, N.; Okuno, Y.; Oe, Y.; Ohta, T. *Chirality* **2019**, *31*, 34−40.
(5) Jang, M.; Kim, S. K.; Lee, J.; Ji, S.; Song, W.; Myung, S.; Lim, J.; Lee, S. S.; Jung, H.-K.; Lee, J.; An, K.-S. *J. Mater. Chem. C* **2019**, *7*, 14504−14510.
(6) Li, H.; Shi, Y.; Han, G.; Liu, J.; Zhang, J.; Li, C.; Yi, Y.; Li, T.; Gao, X.; Di, C.; Huang, J.; Che, Y.; Wang, D.; Hu, W.; Liu, Y.; Jiang, L. *Angew. Chem., Int. Ed.* **2020**, *59*, 4380−4384.
(7) Xie, Q.; Wang, L.; Zhu, Y.; Sun, Q.; Wang, L. *Org. Electron.* **2019**, *74*, 69−76.
(8) Didier, P.; Lobato-Dauzier, N.; Clément, N.; Genot, A. J.; Sasaki, Y.; Leclerc, E.; Minamiki, T.; Sakai, Y.; Fujii, T.; Minami, T. *ChemElectroChem* **2020**, *7*, 1332−1336.
(9) Mano, T.; Nagamine, K.; Ichimura, Y.; Shiwaku, R.; Furusawa, H.; Matsui, H.; Kumaki, D.; Tokito, S. *ChemElectroChem* **2018**, *5*, 3881−3886.
(10) Jang, M.; Kim, H.; Lee, S.; Kim, H. W.; Khedkar, J. K.; Rhee, Y. M.; Hwang, I.; Kim, K.; Oh, J. H. *Adv. Funct. Mater.* **2015**, *25*, 4882−4888.
(11) Li, H.; Shi, W.; Song, J.; Jang, H.-J.; Dailey, J.; Yu, J.; Katz, H. E. *Chem. Rev.* **2019**, *119*, 3−35.
(12) Minami, T.; Sato, T.; Minamiki, T.; Fukuda, K.; Kumaki, D.; Tokito, S. *Biosens. Bioelectron.* **2015**, *74*, 45−48.
(13) Sun, Y.; Wang, Y.; Wu, Y.; Wang, X.; Li, X.; Wang, S.; Xiao, Y. *Anal. Chem.* **2018**, *90*, 9264−9271.
(14) Wang, X.; Wang, Y.; Wu, Y.; Xiao, Y. *Analyst* **2019**, *144*, 2611−2617.
(15) Wu, Y.; Xiao, Y.; Wang, X.; Li, X.; Wang, Y. *ACS Sens.* **2019**, *4*, 2009−2017.
(16) Wu, Y.; Wang, X.; Li, X.; Xiao, Y.; Wang, Y. *Chin. Chem. Lett.* **2020**, *31*, 99−102.
(17) Syu, Y.-C.; Hsu, W.-E.; Lin, C.-T. *ECS J. Solid State Sci. Technol.* **2018**, *7*, Q3196−Q3207.
(18) Song, J.; Dailey, J.; Li, H.; Jang, H.-J.; Russell, L.; Zhang, P.; Searson, P. C.; Wang, J. T.-H.; Everett, A. D.; Katz, H. E. *Adv. Funct. Mater.* **2018**, *28*, 1802605−1802605.
(19) Sadighbayan, D.; Hasanzadeh, M.; Ghafar-Zadeh, E. *TrAC, Trends Anal. Chem.* **2020**, *133*, 116067.
(20) Iskierko, Z.; Checinska, A.; Sharma, P. S.; Golebiewska, K.; Noworyta, K.; Borowicz, P.; Fronc, K.; Bandi, V.; D'Souza, F.; Kutner, W. *J. Mater. Chem. C* **2017**, *5*, 969−977.
(21) Ye, Q.; Guo, L.; Wu, D.; Yang, B.; Tao, Y.; Deng, L.; Kong, Y. *Anal. Chem.* **2019**, *91*, 11864−11871.
(22) Malik, P.; Bhushan, R. *JChS* **2018**, *56*, 92−98.
(23) Sun, H.; Liu, J.; Li, Y.; Wang, J.; Zhang, Y. *J. Chromatogr., B: Anal. Technol. Biomed. Life Sci.* **2019**, *1125*, 10.
(24) Bai, Q.; Zhang, C.; Zhao, Y.; Wang, C.; Maihemuti, M.; Sun, C.; Qi, Y.; Peng, J.; Guo, X.; Zhang, Z.; Fang, L. *Electrophoresis* **2020**, *41*, 1253−1260.
(25) Wang, T.; Wang, Y.; Zhang, Y.; Cheng, Y.; Ye, J.; Chu, Q.; Cheng, G. *J. Chromatogr. A* **2020**, *1625*, 461284.
(26) Guo, L.; Huang, Y.; Zhang, Q.; Chen, C.; Guo, D.; Chen, Y.; Fu, Y. *J. Electrochem. Soc.* **2014**, *161*, B70−B74.
(27) Liu, B.; Zhang, X.; Ding, Y.; Luo, L.; Zhang, F. *Anal. Methods* **2015**, *7*, 3022−3027.
(28) Xuan, C.; Xia, Q.; Xu, J.; Wang, Q.; Lin, X.; Fu, Y. *Anal. Methods* **2016**, *8*, 3564−3569.
(29) Mandal, G.; Bardhan, M.; Ganguly, T. *Colloids Surf., B* **2010**, *81*, 178−184.
(30) Zhu, W.; Li, H.; Wan, A. *J. Fluoresc.* **2019**, *29*, 627−630.
(31) Shankar, S.; Gowthaman, N. S. K.; John, S. A. *J. Electroanal. Chem.* **2018**, *828*, 33−40.
(32) Fang, B.; Ling, Q.; Zhao, W.; Ma, Y.; Bai, P.; Wei, Q.; Li, H.; Zhao, C. *J. Membr. Sci.* **2009**, *329*, 46−55.
(33) Sabatani, E.; Cohen-Boulakia, J.; Bruening, M.; Rubinstein, I. *Langmuir* **1993**, *9*, 2974−2981.
(34) Wang, Y.; Han, Q.; Zhang, Q.; Huang, Y.; Guo, L.; Fu, Y. *J. Solid State Electrochem.* **2013**, *17*, 627−633.
(35) Kim, D.-S.; Park, J.-E.; Shin, J.-K.; Kim, P. K.; Lim, G.; Shoji, S. *Sens. Actuators, B* **2006**, *117*, 488−494.
(36) Chen, C.-P.; Ganguly, A.; Lu, C.-Y.; Chen, T.-Y.; Kuo, C.-C.; Chen, R.-S.; Tu, W.-H.; Fischer, W. B.; Chen, K.-H.; Chen, L.-C. *Anal. Chem.* **2011**, *83*, 1938−1943.
(37) Chi, Z.; Hong, B.; Ren, X.; Cheng, K.; Lu, Y.; Liu, X. *Spectrosc. Lett.* **2018**, *51*, 279−286.
(38) Liu, Y.; Liu, R.; Mou, Y.; Zhou, G. *J. Biochem. Mol. Toxicol.* **2011**, *25*, 95−100.

https://doi.org/10.1021/acs.analchem.1c02460
Anal. Chem. 2021, 93, 14425−14431